1   **Cross-species machine learning improves diagnostic classification of human**

2   **psychiatric disorders**

3   Yafeng Zhan[1,2,†], Jianze Wei[2,3,†], Jian Liang[3], Xiu Xu[4], Ran He[3*], Trevor W. Robbins[5,6],

4   Zheng Wang[1,2,7,8*]

5

6   [1]Institute of Neuroscience, CAS Center for Excellence in Brain Science and Intelligence Technology, State Key

7   Laboratory of Neuroscience, CAS Key Laboratory of Primate Neurobiology, Chinese Academy of Sciences,

8   Shanghai, China

9   [2]University of Chinese Academy of Sciences, China

10   [3]Institute of Automation, CAS Center for Excellence in Brain Science and Intelligence Technology, National

11   Laboratory of Pattern Recognition, Chinese Academy of Sciences, Beijing, China

12   [4]Department of Child Healthcare, Children's Hospital of Fudan University, Shanghai, China

13   [5]Department of Psychology, Behavioural and Clinical Neuroscience Institute, University of Cambridge,

14   Cambridge, UK

15   [6]Institute of Science and Technology for Brain Inspired Intelligence, Fudan University, Shanghai, China

16   [7]Kunming Institute of Zoology, Chinese Academy of Sciences, Kunming, China

17   [8]Shanghai Center for Brain Science and Brain-inspired Intelligence Technology, Shanghai, China

18   [†]These authors contributed equally

19   [*]Correspondence: zheng.wang@ion.ac.cn (Z. W.); rhe@nlpr.ia.ac.cn (R. H.)

20   Tel: +86-(0)21-5492-1713

21   Fax: +86-(0)21-5492-1735

1   **One Sentence Summary:** Features learned from transgenic monkeys enable improved diagnosis of

2   autism-related disorders and dissection of their underlying circuits.

3

1 Abstract

2 Psychiatric disorders often exhibit shared (co-morbid) symptoms, raising controversies over accurate

3 diagnosis and the overlap of their neural underpinnings. Because the complexity of data generated by

4 clinical studies poses a formidable challenge, we have pursued a reductionist framework using brain

5 imaging data of a transgenic primate model of autism spectrum disorder (ASD). Here we report an

6 interpretable cross-species machine learning approach which extracts transgene-related core regions

7 in the monkey brain to construct the classifier for diagnostic classification in humans. The

8 cross-species classifier based on core regions, mainly distributed in frontal and temporal cortex,

9 identified from the transgenic primate model, achieved an accuracy of 82.14% in one clinical ASD

10 cohort obtained from Autism Brain Imaging Data Exchange (ABIDE-I), significantly higher than the

11 human-based classifier (61.31%, $p < 0.001$), which was validated in another independent ASD cohort

12 obtained from ABIDE-II. Such monkey-based classifier generalized to achieve a better classification

13 in obsessive-compulsive disorder (OCD) cohorts, and enabled parsing of differential connections to

14 right ventrolateral prefrontal cortex being attributable to distinct traits in patients with ASD and OCD.

15 These findings underscore the importance of investigating biologically homogeneous samples,

16 particularly in the absence of real-world data adequate for deconstructing heterogeneity inherited in

17 the clinical cohorts.

18

19

Introduction

Comparative analyses of brain connectomics in closely related species can shed light on changes of structural and functional network architecture occurring during evolution (*1-5*), which provides crucial insights for the development of viable diagnostic biomarkers for brain disorders. The pursuit of imaging-based biomarkers for autism spectrum disorder (ASD) has been challenged by a lack of biological accounts (*6*, *7*) and a mix of divergent reports (*8-10*), mainly constrained by its substantial heterogeneity and co-morbidity with other psychiatric disorders such as obsessive-compulsive disorder (OCD) and attention deficit–hyperactivity disorder (ADHD) (*11-14*). Cumulative evidence has demonstrated the feasibility of constructing genetically engineered non-human primates to deepen mechanistic understanding of psychiatric disorders and development of more effective therapeutics (*15-18*). Despite its great potential, there exists no such roadmap for develop methodologies for improving cross-species translational research from direct cross-species extrapolation from monkey results to cross-species translational mapping in the field thus far (*19*).

To this end, we proposed a novel cross-species machine learning framework that leverages connectome-based features learned from a primate genetic model of ASD and then built a classifier for diagnostic utility in humans. We began by postulating what features can be learned from the monkey model that captures the underlying neural pathophysiology likely shared with human ASD patients. Within the network graph setting (*4*), two basic elements of brain circuitry: nodes (brain regions) and interconnecting edges (connections between pairs of nodes) are considered (*1*, *4*, *20*). Our intuition was that characteristics of nodes are more likely to be evolutionarily conserved between the primate species, given substantial variations of edges subserving species-specific

4

1   behavioral and cognitive adaptations (*1*, *4*). Moreover, supposing that only a subset of brain regions

2   (not the entire brain) are particularly relevant to the core neuropathology of autism (termed as "core

3   regions" thereafter) (*9*, *21*), we deduced that only these "core regions" are useful for greatly reducing

4   the complexity of cross-species mapping of this framework (Fig. 1A).

5   Using whole-brain functional connectivity datasets obtained from wild-type and human

6   Methyl-CpG binding protein 2 (MECP2) transgenic monkeys (*17*), and from multicenter ASD

7   databases, available from the Autism Brain Imaging Data Exchange (ABIDE-I, N = 1112; ABIDE-II,

8   N = 1114) (*8*, *22*), OCD (N = 186) (*23*), and ADHD publicly available from ADHD-200 (N = 776)

9   (*24*), we aim to test two specific hypotheses: (i) whether the monkey-based features (core regions)

10   can improve the diagnosis accuracy of the ASD cohort; (ii) whether these monkey-based features can

11   be generalised to improve the discriminative classification of OCD and ADHD from their healthy

12   controls (HCs). To further parse the biological accounts of the monkey-based classifiers, stepwise

13   linear regression models based on these classifiers are built to predict clinical measures of symptom

14   severity of psychiatric patients (Fig. 1).

15

Results

17   A total of 144 fMRI datasets from 5 *MECP2* transgenic (TG) and 11 wild-type (WT) monkeys were

18   collected. We also analyzed ASD data from ABIDE-I/II repository (*8*, *22*) and ADHD cohort from

19   ADHD-200 (*24*), two publicly available multisite datasets of resting-state functional imaging data,

20   and one OCD cohort from our institutional database (*25*).

1   Core regions mapping between primate species

2   In order to determine the core regions in the monkey datasets for use in cross-species mapping, we

3   adopted the sparse linear regression model based on the group lasso penalty (*26*, *27*) which selects

4   groups of variables (regions) based on predefined variable groups (all edges connected to one region

5   being treated as a group, i.e. rows in an adjacency matrix). The penalty is deployed to regularize the

6   problem to impose a network structure, i.e., core regions versus non-relevant regions here (Fig. 1B, see

7   Materials and Methods for details of the group lasso method). A total of 144 fMRI datasets from 5

8   *MECP2* transgenic (TG) and 11 wild-type (WT) monkeys (Table S1) were used to construct the

9   connectivity network using 94 parcellated brain regions (see Table S2 for a complete list of anatomical

10   labels) for each dataset. The group lasso algorithm automatically and objectively identified 9 core

11   regions out of 94 nodes of the monkey brain, which are the left central temporal cortex (CTC), right

12   superior temporal cortex (STG), right dorsolateral prefrontal cortex (dlPFC), right primary

13   somatosensory cortex (S1) and right primary motor cortex (M1), left anterior cingulate cortex (ACC),

14   right centrolateral prefrontal cortex (clPFC), left superior parietal cortex (SPL), right ventrolateral

15   prefrontal cortex (vlPFC) (Fig. 2A). To assess the biological significance of these core regions, a two

16   sample *t*-test of node strength, i.e. the sum of functional connnectivities of all edges connecting this

17   node was performed between TG and WT groups. Relative to WT group, the TG group exhibited

18   significantly increased node strength in right vlPFC ($p = 0.004$*, * means FDR corrected for multiple

19   comparisons thereinafter), left ACC ($p = 0.008$*), right clPFC ($p = 0.001$*) and right dlPFC ($p = $

20   0.004*) (Fig. 2B). In contrast, the right S1 ($p = 0.002$*) and right M1 ($p = 0.025$) showed decreased

21   node strength in TG group (Fig. 2B). In addition, the correlation analyses between node strength and

1   phenotypic behaviors observed in transgenic monkeys, measured by time in repetitive circular routing

2   and locomotion (*17, 28*), revealed a significant negative relationship between the right vlPFC and

3   circular routing (r = -0.932, p = 0.021) and between left STG and locomotion (r = -0.922, p = 0.026)

4   (Fig. S1). Conversely, the node strength of left ACC was positively associated with relative circular

5   routing in TG group (r = 0.910, p = 0.032) (Fig. S1).

6

7   **Highly accurate monkey-based classifier for ASD**

8   Applying these 9 core regions to the human connectomics datasets, a functional-connection (FC),

9   monkey-based classifier was constructed (there are a total of 801 FCs based on these 9 regions) (Fig.

10   1D). For diagnostic tests, 133 subjects with ASD and demographically matched 203 healthy controls

11   (HC) were used from a total of 1112 subjects in ABIDE-I (*8*), and 60 subjects with ASD and 89

12   matched HC were used from 1114 subjects in ABIDE-II (*22*) after basic demographic and diagnostic

13   screening. Using the standard lasso with a 10 × 10 nested cross-validation (*29*), we determined a

14   subset of relevant, non-redundant edge features among the 801 FCs for use in classification. Note that

15   the test set was never used for validation or feature selection (Fig. 1D; Fig. S2). A sparse logistic

16   regression (*30*) in tandem with leave-one-participant-out cross validation was subsequently

17   implemented to classify patients with ASD from HC in ABIDE-I cohort (Fig. 1E; Fig. S2), and was

18   achieved with a cross-validated accuracy of 82.14% (Permutation test p = 0.001, Fig. S3; 95%

19   confidence interval (CI), 77.53% to 86.00%), sensitivity of 79.70% (95% CI, 71.66% to 85.98%) and

20   specificity of 83.74% (95% CI, 77.78% to 88.40%), corresponding to the area under the receiver

21   operating characteristic (ROC) curve (AUC) of 0.884 (Fig. 2C; Table S3). In the independent

1   ABIDE-II cohort, the monkey-based classifier also achieved remarkable performance with an

2   accuracy of 75.17% (Permutation test $p = 0.014$, Fig. S3; 95% CI, 67.30% to 81.71%), sensitivity of

3   70.00% (95% CI, 56.63% to 80.80%), specificity of 78.65% (95% CI, 68.43% to 86.35%), and the

4   AUC was 0.769 (Fig. 2D; Table S3).

5   We applied the same group lasso algorithm to one human ASD cohort to identify core regions,

6   and used them to construct a classifier for classification in other ASD cohorts. Namely, the group

7   lasso penalty was applied to identify core regions in one human ASD cohort, which were then used to

8   construct the classifier for diagnostic classification in another human ASD cohort, and vice versa. In

9   the ABIDE-II data set, we identified core regions as the left STG, left dorsal part of anterior visual

10   area (VACd), left Visual area 2 (V2), right M1, bilateral ACC, right clPFC, right vlPFC, and right

11   globus pallidus (GP) (Fig. S4). The classifier based on these core regions achieved an accuracy of

12   61.31% (95% CI, 55.85% to 66.51%), sensitivity of 56.39% (95% CI, 47.53% to 64.88%),

13   specificity of 64.53% (95% CI, 57.49% to 71.02%) and AUC of 0.644 in the ABIDE-I cohort (Fig.

14   2C; Table S3), which is significantly lower than that of the monkey-based classifier ($p < 0.001$,

15   McNemar's test, Table S3) (*31*). By contrast, core regions identified in the ABIDE-I cohort were the

16   left thalamus (THa), right primary visual area (V1), right V2 and right STG (Fig. S4). These

17   ABIDE-I based classifier achieved an accuracy of 60.40% (95% CI, 52.04% to 68.21%) with a

18   sensitivity of 53.33% (95% CI, 40.10% to 66.14%), specificity of 65.17% (95% CI, 54.26% to

19   74.76%) and AUC of 0.611 in the ABIDE-II cohort, which is significantly lower than that of the

20   monkey-based classifier ($p = 0.003$, Fig. 2D; Table S3). Furthermore, we asked whether this

21   monkey-based classifier would outperform random choice (by chance), i.e., randomly picking 9 out

1   of 94 nodes as 'core regions'. We repeated the above monkey-based classifier analysis through using

2   a random selection of 9 regions and constructing the corresponding classifier to distinguish ASD

3   from HC. This was repeated 5,000 times to assess the probability of attaining better accuracy than

4   the actual monkey-based classifier. We observed that the performance of the monkey-based classifier

5   was significantly better than chance for the ABIDE-I ($p = 0.0002$, Fig. 2G) and -II cohorts ($p = 0.052$,

6   Fig. 2H). Note that there are some random selections showing higher accuracy than the

7   monkey-based classifier (Fig. 2G,H). Upon closer examination, we found that a random selection of

8   9 regions outperforms the monkey-based one in one cohort whereas it always fails to achieve

9   reasonable performance in other cohorts, indicating poor generalizability for the random choices of

10   core regions (Fig. S5).

11

12   Application of the monkey-based classifier to other human disorders

13   We next tested the generalizability of the monkey-based classifier in OCD and ADHD datasets. The

14   OCD cohort contained 92 OCD patients and 79 healthy controls which were recruited through the

15   local department of the OCD Clinic at Ruijin Hospital and part of this data set has recently been

16   published elsewhere (*23*). The ADHD cohort that included 102 subjects with ADHD and 173

17   demographically matched HC was enrolled from a public ADHD-200 sample which provides a total

18   of 776 subjects including 285 ADHD patients and 491 HC (*24*). In this OCD cohort, the classifier

19   based on the same set of core regions from the monkey model achieve a remarkable performance

20   with an accuracy of 78.36% (Permutation test $p = 0.002$, Fig. S3; 95% CI, 71.29% to 84.13%),

21   sensitivity of 73.91% (95% CI, 63.53% to 82.26%), specificity of 83.54% (95% CI, 73.14% to

1   90.61%) and AUC of 0.848 (Fig. 2E), which outperformed other two human-based classifiers

2   (ABIDE-I, $p = 0.044$; ABIDE-II, $p = 0.000$; Table S3), and the randomization classifiers ($p = 0.047$,

3   Fig. 2I). However, in the ADHD cohort, the monkey-based classifier performed with an accuracy of

4   64.73% (95% CI, 58.73% to 70.31%), sensitivity = 51.96% (95% CI, 41.90% to 61.88%), specificity

5   = 72.25% (95% CI, 64.85% to 78.65%) and AUC = 0.662, which yielded no significant difference

6   relative to other human-based classifiers (Fig. 2F; Table S3). Notably core regions identified in the

7   monkey model showed better generalizability than randomly-generated ones in ASD and OCD (Fig.

8   S5).

9

10 **Characteristics of nodes and edges in the monkey-based classifier for ASD and**

11 **OCD**

12 We proceeded to quantitatively evaluate the relation between key elements (nodes and edges) of the

13 monkey-based classifier and clinical symptoms in ASD and OCD. The SLR algorithm automatically

14 identified 101, 74 and 64 FCs from the ABIDE-I, ABIDE-II and OCD data sets for reliable

15 classification of patients and HCs, respectively (Fig. 3A-C). We characterized the spatial profiles of

16 these FCs by calculating their intra-lobe and inter-lobe proportional distribution (Fig. 3D-F).

17 Analysis of the spatial distribution of these classifiers shows that both ASD and OCD shared

18 discriminant features of intra-lobe FCs mostly within the prefrontal lobe, whereas fronto-temporal and

19 fronto-subcortical connections significantly epitomize their overall differences (Fig. 3G). In 48 of 60

20 participants with research-reliable Autism Diagnostic Observation Schedule (ADOS) scores from the

21 ABIDE-II cohort, we found that node strengths of the right vlPFC ($r = -0.333$, $p = 0.021$), left CTC (r

1   = -0.308, p = 0.033), right STG (r = -0.336, p = 0.020) and right S1 (r = -0.315, p = 0.029) exhibited

2   significant correlations with the communication sub-scores of the ADOS (ADOS COMM) in patients

3   (Fig. 4A; Table S4). Negative correlations between the node strengths of left ACC (r = -0.295, p =

4   0.042) and right dlPFC (r = -0.291, p = 0.045) and the ADOS COMM scores were also found in these

5   ASD patients (Table S4). The node strength of the right vlPFC was found associated with Yale-Brown

6   Obsessive Compulsive Scale (Y-BOCS) scores in OCD patients (r = -0.217, p = 0.038, Fig. 4A). In

7   addition, we found a significant association between the HAM-A scores of OCD patients and the node

8   strength of right SPL (r = -0.237, p = 0.023).

9   For those regions exhibiting significant correlations with symptom severity scores, we performed

10   a stepwise linear regression to predict symptom severity by modeling the relationship between the

11   dependent variable (clinical symptom measurements) and the independent variables (FCs connected

12   to a specific core region), which allowed determination of whether individual nodes and edges of the

13   classifiers were commonly shared or uniquely linked to symptomatic domains of ASD and OCD. For

14   instance, the FCs connecting to one core region such as the right vlPFC among all identified FCs

15   were used to predict the ADOS COMM scores of ASD patients. Pearson's correlation coefficient was

16   used to evaluate the performance of the linear model in predicting symptom severity. The linear

17   model based on the connection of right vlPFC-right THa achieved a correlation of r = 0.437 (p =

18   0.002*) between predicted and measured ADOS COMM scores in patients with ASD in the ABIDE-II

19   group (r = 0.437, p = 0.002*, Fig. 4B; Table S5). The linear model is expressed as follows:

$$ADOS\ COMM = 3.96 - 2.06 \times (vlPFC.R{\sim}THa.R)$$

20   In fact, the ADOS COMM score was significantly predicted by connections between right dlPFC and

1   left STG, right STG and right orbitolateral prefrontal cortex (lOFC), right S1 and left dorsomedial

2   prefrontal cortex (dmPFC), between left ACC and both left medial parietal cortex (mPC) and left STG

3   (Fig. 4B). By contrast, FC between right vlPFC and right prefrontal polar cortex (PFCpol) was

4   predictive of the measured Y-BOCS scores of OCD patients ($r = 0.219$, $p = 0.036$*, Fig. 4C; Table S5):

$$Y - BOCS = 31.86 - 5.07 \times (vlPFC.R{\sim}PFCpol.R)$$

5   Of all left SPL-linked connections, the predicted HAM-A scores based on the FC between left SPL

6   and left CTC was significantly correlated with the actual HAM-A scores of these OCD patients ($r =$

7   0.281, $p = 0.007$*, Fig. 4C; Table S5).

8

Discussion

10   The superior predictive performance of the monkey-based model speaks to the value of investigating

11   biologically homogeneous samples, particularly in the absence of sufficient real-world data available

12   for deconstructing heterogeneity inherited in the clinical cohorts (given the overwhelming

13   dimensions in most neuroimaging settings) (32). We have demonstrated that this particular set of

14   core regions, although identified in a relatively small number of transgenic monkeys, is sufficiently

15   powerful to set the stage for cross-species mapping and prioritization of features for reducing clinical

16   heterogeneity. This is probably because predisposition of a single genetic manipulation in animal

17   models can be highly susceptible to specific neural circuits/pathways, revealing the extent of a

18   tangible circuit endophenotype and its manifestation at the behavioral domain (33). Fortunately, we

19   managed to unravel a circuit-level path to successfully map key nodes in the pathological circuits of

20   transgenic monkeys to the homologs in various human conditions, strongly suggesting an

1   evolutionarily conserved mechanism of core regions in the functional specialization of large-scale

2   brain networks.

3   Importantly, the present machine learning framework enables the search for some

4   straightforward explanations for how a neural circuit allows superior classification for different

5   human cohorts, and thus to gain illuminating insights into the mechanisms by which these features

6   were linked to the etiology of ASD and OCD. This is illustrated by the fact that the core regions,

7   mostly distributed in frontal and temporal lobes including right vlPFC right STG, were correlated

8   with social communicative deficits (*9, 21, 34*). The right vlPFC and left ACC play an important role

9   in the "stop circuit" (*35, 36*), heavily implicated in relation to restricted, repetitive behaviors and

10 interests in ASD (*37*). Moreover, the FC between left SPL and left CTC predicted the severity of

11 anxiety, and the relation between anxiety and attention in OCD (*38*). Additionally, our findings

12 highlight the crucial role of two core regions S1 and M1, indicating their attributes to motor

13 impairment in ASD (*39*) and impaired social-communicative skill development (*39, 40*), as deficits in

14 S1 may affect the ability to master motor skills (*41*). Since sensory and motor disturbances have been

15 hypothesized as some of the earliest signs of abnormality in children with ASD (*40*), future studies

16 characterizing the trajectory of sensorimotor disturbance and the "downstream" effects onto social

17 and communicative interaction in later development would be invaluable for addressing the

18 mechanistic basis of symptomatic domains in autistic children.

19   From a circuit perspective, these core regions may simultaneously function as critical hubs to

20 form differential patterns of functional coupling with the rest of the brain that underlie distinct

21 clinical-symptom profiles in a variety of diseases. Upon close inspection, ASD-specific features

13

1   exhibit apparently marked distribution of fronto-temporal and fronto-parietal connections,

2   prominently involved in cognitive control and social communication (*42*). By contrast,

3   dysconnectivity of OCD shows a significant bias towards the fronto-subcortical pathways, largely

4   involved in response inhibition and cognitive flexibility (*9*, *35*). Furthermore, a dissection of two

5   distinct vlPFC-centered circuits from the monkey-based classifier has revealed dual

6   neuropathology-dependent roles for the vlPFC which not only contributes to the communication

7   domain of ASD but also to the compulsivity of OCD, thus emphasizing both unitary and diverse

8   features contributing to the aetiological overlap between these disorders (*14*, *35*).

9   This is to our knowledge the first study to propose this cross-species machine learning method for

10   defining circuit endophenotypes and parsing heterogeneity and complexity across mental disorders, so

11   caution is warranted. Replication to validate the present predictive algorithm with data from other

12   populations and settings will be critical to extend the current use of genetically-engineered animal

13   models to broader human application scenarios. Intriguingly, the combination of the 9 core regions

14   pre-identified in transgenic monkeys effectively tease out relevant functional connections to achieve

15   desirable performance compared to randomly-generated combinations (Fig. 2G-I), which calls for

16   future biological validation regarding the role of the 9 core regions combination in the circuit

17   pathology underlying both ASD and OCD and their potential utility in other disorders such as

18   schizophrenia and addiction.

19   In summary, despite the heterogeneous genetic architecture of ASD and related disorders, the

20   present translational strategy coupled with machine learning algorithms attests to the construct

21   validity and feasibility of using genetically modified non-human primates to study human brain

1 diseases, with important implication for parsing biologically-defined circuit endophenotypes that

2 transcend conventional diagnostic boundaries in mental disorders. Nevertheless, the proposed

3 interspecies framework can serve as a general strategy for bridging gaps between diagnostic categories

4 of complex brain diseases, genetic and circuit mechanisms, thereby facilitating the development of

5 targeted therapies based on symptom-specific mechanisms.

6

Supplementary Materials

8 Materials and Methods

9 Supplementary References

10 Fig S1. Correlation between node strength of core regions and behavior abnormalities in TG group

11 Fig. S2. Illustration of nested 10×10 feature selection and leave-one-out cross-validation

12 Fig. S3. Null distribution of classification accuracy in the permutation test

13 Fig. S4. Identified core regions using ABIDE-I and ABIDE-II datasets

14 Fig. S5. Plots depicting the poor generalizability of random selections of 9 core regions in different

15 cohorts

16 Table S1. Characteristics of all TG and WT monkeys

17 Table S2. Cortical and subcortical parcellation and abbreviations

18 Table S3. Classification performance of classifiers based on different sets of core regions

19 Table S4. Correlations between node strength and symptom severity in ASD and OCD cohorts

20 Table S5. Prediction of symptom severity using functional connections identified in the classifier

21 Table S6. Characteristics of human ABIDE-I cohorts

1   Table S7. Characteristics of human ABIDE-II cohorts

2   Table S8. Characteristics of human OCD cohorts

3   Table S9. Characteristics of human ADHD cohorts

4   Table S10. Imaging protocols for resting-state fMRI used in the present study

5

References

1. R. B. Mars, S. N. Sotiropoulos, R. E. Passingham, J. Sallet, L. Verhagen, A. A. Khrapitchev, N. Sibson, S. Jbabdi, Whole brain comparative anatomy using connectivity blueprints. *eLife* **7**, (2018).

2. J. K. Rilling, M. F. Glasser, T. M. Preuss, X. Ma, T. Zhao, X. Hu, T. E. Behrens, The evolution of the arcuate fasciculus revealed with comparative DTI. *Nat. Neurosci.* **11**, 426-428 (2008).

3. C. J. Donahue, M. F. Glasser, T. M. Preuss, J. K. Rilling, D. C. Van Essen, Quantitative assessment of prefrontal cortex in humans relative to nonhuman primates. *Proc. Natl. Acad. Sci. U. S. A.* **115**, E5183-E5192 (2018).

4. M. P. van den Heuvel, E. T. Bullmore, O. Sporns, Comparative Connectomics. *Trends Cogn Sci* **20**, 345-361 (2016).

5. D. Mantini, U. Hasson, V. Betti, M. G. Perrucci, G. L. Romani, M. Corbetta, G. A. Orban, W. Vanduffel, Interspecies activity correlations reveal functional correspondence between monkey and human brain areas. *Nature methods* **9**, 277-282 (2012).

6. A. Abi-Dargham, G. Horga, The search for imaging biomarkers in psychiatric disorders. *Nat. Med.* **22**, 1248-1255 (2016).

7. M. Sahin, M. Sur, Genes, circuits, and precision therapies for autism and related neurodevelopmental disorders. *Science* **350**, (2015).

8. A. Di Martino, C. G. Yan, Q. Li, E. Denio, F. X. Castellanos, K. Alaerts, J. S. Anderson, M. Assaf, S. Y. Bookheimer, M. Dapretto, B. Deen, S. Delmonte, I. Dinstein, B. Ertl-Wagner, D. A. Fair, L. Gallagher, D. P. Kennedy, C. L. Keown, C. Keysers, J. E. Lainhart, C. Lord, B. Luna, V.

17

Menon, N. J. Minshew, C. S. Monk, S. Mueller, R. A. Muller, M. B. Nebel, J. T. Nigg, K. O'Hearn, K. A. Pelphrey, S. J. Peltier, J. D. Rudie, S. Sunaert, M. Thioux, J. M. Tyszka, L. Q. Uddin, J. S. Verhoeven, N. Wenderoth, J. L. Wiggins, S. H. Mostofsky, M. P. Milham, The autism brain imaging data exchange: towards a large-scale evaluation of the intrinsic brain architecture in autism. *Mol. Psychiatry* **19**, 659-667 (2014).

9. C. Ecker, S. Y. Bookheimer, D. G. Murphy, Neuroimaging in autism spectrum disorder: brain structure and function across the lifespan. *Lancet Neurol.* **14**, 1121-1134 (2015).

10. A. Hahamy, M. Behrmann, R. Malach, The idiosyncratic brain: distortion of spontaneous connectivity patterns in autism spectrum disorder. *Nat. Neurosci.* **18**, 302-309 (2015).

11. E. Simonoff, A. Pickles, T. Charman, S. Chandler, T. Loucas, G. Baird, Psychiatric disorders in children with autism spectrum disorders: prevalence, comorbidity, and associated factors in a population-derived sample. *J. Am. Acad. Child Adolesc. Psychiatry* **47**, 921-929 (2008).

12. S. S. Jeste, D. H. Geschwind, Disentangling the heterogeneity of autism spectrum disorder through genetic findings. *Nat. Rev. Neurol.* **10**, 74-81 (2014).

13. C. O. Carlisi, L. J. Norman, S. S. Lukito, J. Radua, D. Mataix-Cols, K. Rubia, Comparative Multimodal Meta-analysis of Structural and Functional Brain Abnormalities in Autism Spectrum Disorder and Obsessive-Compulsive Disorder. *Biol. Psychiatry* **82**, 83-102 (2017).

14. T. W. Robbins, C. M. Gillan, D. G. Smith, S. de Wit, K. D. Ersche, Neurocognitive endophenotypes of impulsivity and compulsivity: towards dimensional psychiatry. *Trends Cogn Sci* **16**, 81-91 (2012).

15. C. G. Jennings, R. Landman, Y. Zhou, J. Sharma, J. Hyman, J. A. Movshon, Z. Qiu, A. C.

Roberts, A. W. Roe, X. Wang, H. Zhou, L. Wang, F. Zhang, R. Desimone, G. Feng, Opportunities and challenges in modeling human brain disorders in transgenic primates. *Nat. Neurosci.* **19**, 1123-1130 (2016).

16. J. C. Izpisua Belmonte, E. M. Callaway, S. J. Caddick, P. Churchland, G. Feng, G. E. Homanics, K. F. Lee, D. A. Leopold, C. T. Miller, J. F. Mitchell, S. Mitalipov, A. R. Moutri, J. A. Movshon, H. Okano, J. H. Reynolds, D. Ringach, T. J. Sejnowski, A. C. Silva, P. L. Strick, J. Wu, F. Zhang, Brains, genes, and primates. *Neuron* **86**, 617-631 (2015).

17. Z. Liu, X. Li, J. T. Zhang, Y. J. Cai, T. L. Cheng, C. Cheng, Y. Wang, C. C. Zhang, Y. H. Nie, Z. F. Chen, W. J. Bian, L. Zhang, J. Xiao, B. Lu, Y. F. Zhang, X. D. Zhang, X. Sang, J. J. Wu, X. Xu, Z. Q. Xiong, F. Zhang, X. Yu, N. Gong, W. H. Zhou, Q. Sun, Z. Qiu, Autism-like behaviours and germline transmission in transgenic monkeys overexpressing MeCP2. *Nature* **530**, 98-102 (2016).

18. Y. Chen, J. Yu, Y. Niu, D. Qin, H. Liu, G. Li, Y. Hu, J. Wang, Y. Lu, Y. Kang, Y. Jiang, K. Wu, S. Li, J. Wei, J. He, J. Wang, X. Liu, Y. Luo, C. Si, R. Bai, K. Zhang, J. Liu, S. Huang, Z. Chen, S. Wang, X. Chen, X. Bao, Q. Zhang, F. Li, R. Geng, A. Liang, D. Shen, T. Jiang, X. Hu, Y. Ma, W. Ji, Y. E. Sun, Modeling Rett Syndrome Using TALEN-Edited MECP2 Mutant Cynomolgus Monkeys. *Cell* **169**, 945-955 e910 (2017).

19. R. Pryluk, Y. Kfir, H. Gelbard-Sagiv, I. Fried, R. Paz, A Tradeoff in the Neural Code across Regions and Species. *Cell* **176**, 597-609 e518 (2019).

20. J. Pu, J. Wang, W. Yu, Z. Shen, Q. Lv, K. Zeljic, C. Zhang, B. Sun, G. Liu, Z. Wang, Discriminative Structured Feature Engineering for Macroscale Brain Connectomes. *IEEE*

Trans. Med. Imaging **34**, 2333-2342 (2015).

21. D. G. Amaral, C. M. Schumann, C. W. Nordahl, Neuroanatomy of autism. *Trends Neurosci.* **31**, 137-145 (2008).

22. A. Di Martino, D. O'Connor, B. Chen, K. Alaerts, J. S. Anderson, M. Assaf, J. H. Balsters, L. Baxter, A. Beggiato, S. Bernaerts, L. M. Blanken, S. Y. Bookheimer, B. B. Braden, L. Byrge, F. X. Castellanos, M. Dapretto, R. Delorme, D. A. Fair, I. Fishman, J. Fitzgerald, L. Gallagher, R. J. Keehn, D. P. Kennedy, J. E. Lainhart, B. Luna, S. H. Mostofsky, R. A. Muller, M. B. Nebel, J. T. Nigg, K. O'Hearn, M. Solomon, R. Toro, C. J. Vaidya, N. Wenderoth, T. White, R. C. Craddock, C. Lord, B. Leventhal, M. P. Milham, Enhancing studies of the connectome in autism using the autism brain imaging data exchange II. *Sci Data* **4**, 170010 (2017).

23. D. Yin, C. Zhang, Q. Lv, X. Chen, K. Zeljic, H. Gong, S. Zhan, H. Jin, Z. Wang, B. Sun, Dissociable Frontostriatal Connectivity: Mechanism and Predictor of the Clinical Efficacy of Capsulotomy in Obsessive-Compulsive Disorder. *Biol. Psychiatry*,   (2018).

24. H. D. Consortium, The ADHD-200 Consortium: A Model to Advance the Translational Potential of Neuroimaging in Clinical Neuroscience. *Front. Syst. Neurosci.* **6**, 62 (2012).

25. D. Yin, C. Zhang, Q. Lv, X. Chen, K. Zeljic, H. Gong, S. Zhan, H. Jin, Z. Wang, B. Sun, Dissociable Frontostriatal Connectivity: Mechanism and Predictor of the Clinical Efficacy of Capsulotomy in Obsessive-Compulsive Disorder. *Biol. Psychiatry* **84**, 926-936 (2018).

26. M. Yuan, Y. Lin, Model selection and estimation in regression with grouped variables. *J Roy Stat Soc B* **68**, 49-67 (2006).

27. J. Wang, P. Wonka, J. P. Ye, Lasso screening rules via dual polytope projection. *J. Mach. Learn.*

Res. **16**, 1063-1101 (2015).

28. D. C. Cai, Z. W. Wang, T. T. Bo, S. Y. Yan, Y. L. Liu, Z. W. Liu, K. Zeljic, X. Y. Chen, Y. F. Zhan, X. Xu, Y. S. Du, Y. W. Wang, J. Cang, G. Z. Wang, J. Zhang, Q. Sun, Z. L. Qiu, S. J. Ge, Z. Ye, Z. Wang, MECP2 duplication causes aberrant GABA pathways, circuits and behaviors in transgenic monkeys: neural mappings to patients with autism. *bioRxiv*, 728113 (2019).

29. R. Tibshirani, Regression shrinkage and selection via the Lasso. *J Roy Stat Soc B Met* **58**, 267-288 (1996).

30. O. Yamashita, M. A. Sato, T. Yoshioka, F. Tong, Y. Kamitani, Sparse estimation automatically selects voxels relevant for the decoding of fMRI activity patterns. *Neuroimage* **42**, 1414-1429 (2008).

31. Q. McNemar, Note on the Sampling Error of the Difference between Correlated Proportions or Percentages. *Psychometrika* **12**, 153-157 (1947).

32. M. V. Lombardo, M. C. Lai, S. Baron-Cohen, Big data approaches to decomposing heterogeneity across the autism spectrum. *Mol. Psychiatry*, (2019).

33. A. Krol, R. D. Wimmer, M. M. Halassa, G. Feng, Thalamic Reticular Dysfunction as a Circuit Endophenotype in Neurodevelopmental Disorders. *Neuron* **98**, 282-295 (2018).

34. L. T. Eyler, K. Pierce, E. Courchesne, A failure of left temporal cortex to specialize for language is an early emerging and fundamental property of autism. *Brain* **135**, 949-960 (2012).

35. A. R. Aron, T. W. Robbins, R. A. Poldrack, Inhibition and the right inferior frontal cortex: one decade on. *Trends Cogn Sci* **18**, 177-185 (2014).

36. J. W. Dalley, B. J. Everitt, T. W. Robbins, Impulsivity, compulsivity, and top-down cognitive

1   control. *Neuron* **69**, 680-694 (2011).

2 37. K. N. Thakkar, F. E. Polli, R. M. Joseph, D. S. Tuch, N. Hadjikhani, J. J. Barton, D. S. Manoach,

3   Response monitoring, repetitive behaviour and anterior cingulate abnormalities in autism

4   spectrum disorders (ASD). *Brain* **131**, 2464-2478 (2008).

5 38. A. P. Pacheco-Unguetti, A. Acosta, A. Callejas, J. Lupianez, Attention and anxiety: different

6   attentional functioning under state and trait anxiety. *Psychol. Sci.* **21**, 298-304 (2010).

7 39. A. Thompson, D. Murphy, F. Dell'Acqua, C. Ecker, G. McAlonan, H. Howells, S.

8   Baron-Cohen, M. C. Lai, M. V. Lombardo, M. A. Consortium, C. Marco, Impaired

9   Communication Between the Motor and Somatosensory Homunculus Is Associated With Poor

10   Manual Dexterity in Autism Spectrum Disorder. *Biol. Psychiatry* **81**, 211-219 (2017).

11 40. C. E. Robertson, S. Baron-Cohen, Sensory perception in autism. *Nat. Rev. Neurosci.* **18**,

12   671-684 (2017).

13 41. M. B. Nebel, A. Eloyan, C. A. Nettles, K. L. Sweeney, K. Ament, R. E. Ward, A. S. Choe, A. D.

14   Barber, J. J. Pekar, S. H. Mostofsky, Intrinsic Visual-Motor Synchrony Correlates With Social

15   Deficits in Autism. *Biol. Psychiatry* **79**, 633-641 (2016).

16 42. W. Cheng, E. T. Rolls, H. Gu, J. Zhang, J. Feng, Autism: reduced connectivity between cortical

17   areas involved in face expression, theory of mind, and the sense of self. *Brain* **138**, 1382-1393

18   (2015).

19

1

Figure legend

3

Fig. 1. Schematic of a cross-species machine learning framework.

(A) Illustration of a cross-species circuit mapping strategy, which is formulated on the basis of the

1   intuition that characteristics of the brain circuitry between nonhuman and human primates are

2   evolutionarily conserved at the node or edge level.

3   (B) Using a group lasso to identify core regions in transgenic monkeys

4   (C) Associations between characteristics of core regions and behavior abnormalities in transgenic

5   monkeys.

6   (D) Feature engineering in the human data is initiated by a one-to-one projection of core regions from

7   monkey to human and then subjected to a nested 10-fold feature selection for use in human

8   classification.

9   (E) Optimal features were input into the sparse logistic regression (SLR) procedure for human

10   classification.

11   (F) Spatial profiles of the identified FCs in the ASD and OCD classifiers.

12   (G) Associations between characteristics of nodes and edges in the ASD and OCD classifiers and

13   symptom severity in patients.
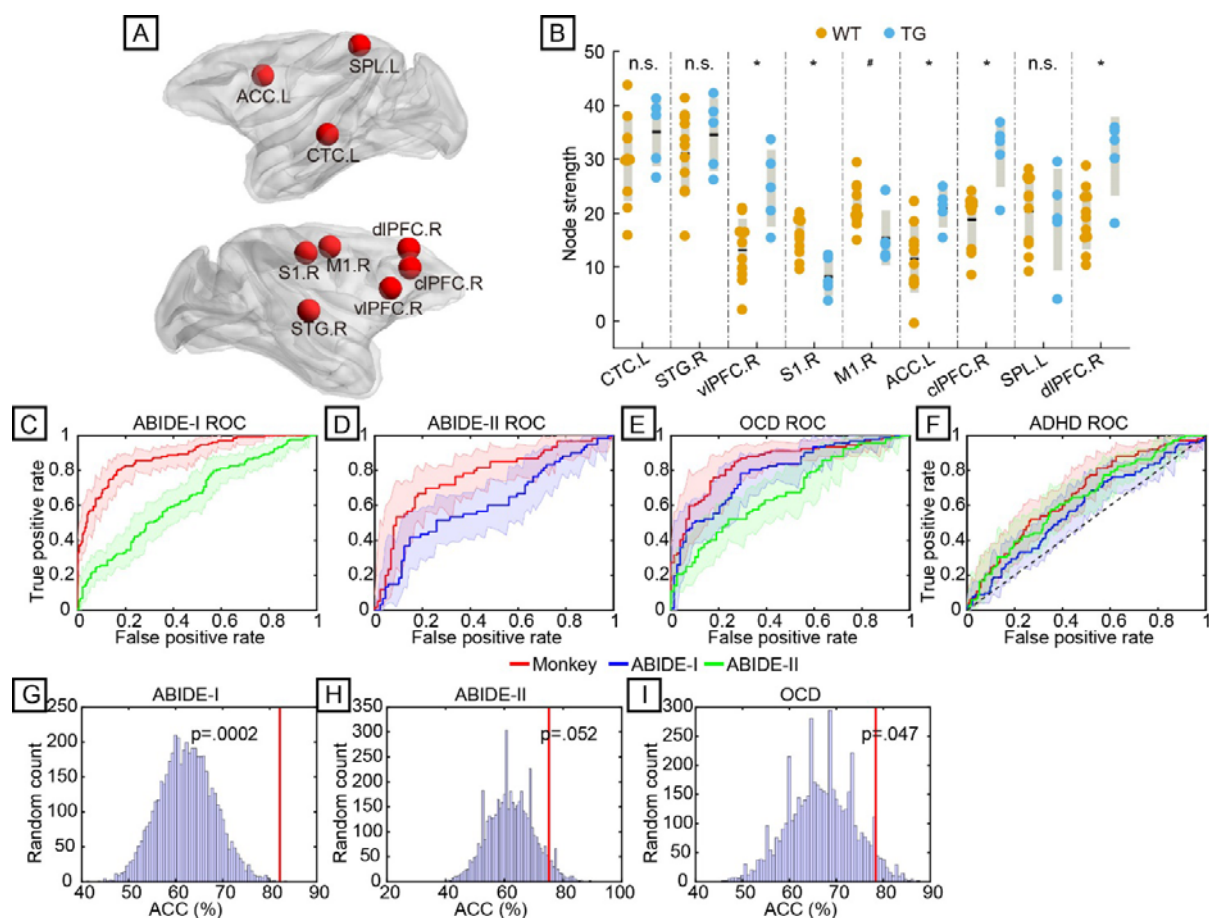
Fig. 2. Performance of diagnostic classification for ASD and OCD cohorts using the monkey-/human-based classifiers.

(A) Spatial distribution of 9 core regions identified from the monkey datasets.

(B) Node strength of the 9 core regions in TG ($n = 5$, blue dots) compared with WT monkey ($n = 11$, yellow dots) using two sample t-test. Relative to WT group, the TG group exhibited significantly increased node strength in right vlPFC, left ACC, right clPFC and right dlPFC, whereas decreased node strength in right S1 and right M1. A black line denotes the group-averaged node strength and gray shading denotes standard deviation. * indicates $p < 0.05$, FDR corrected; # indicates $p < 0.05$, uncorrected; n.s., not significant.

1   (C-F) Receiver operating characteristic (ROC) curves of the monkey-based classifier are plotted with

2   those of the human-based classifier in ABIDE-I (C), ABIDE-II (D), OCD (E) and ADHD dataset (F),

3   respectively. Red, blue and green lines denote ROC curves of the monkey-, the ABIDE-I and the

4   ABIDE-II based classifier, respectively; shaded area indicates a 95% confidence interval.

5   (G-I) Accuracy histograms of cross-validation by using randomly-generated core regions to construct

6   the classifier in two ASD datasets and one OCD dataset. The vertical red lines indicate the

7   classification accuracy achieved by the monkey-based classifier, which reaches a statistical

8   confidence level at $p = 0.0002$ (G), $p = 0.052$ (H), and $p = 0.047$ (I).
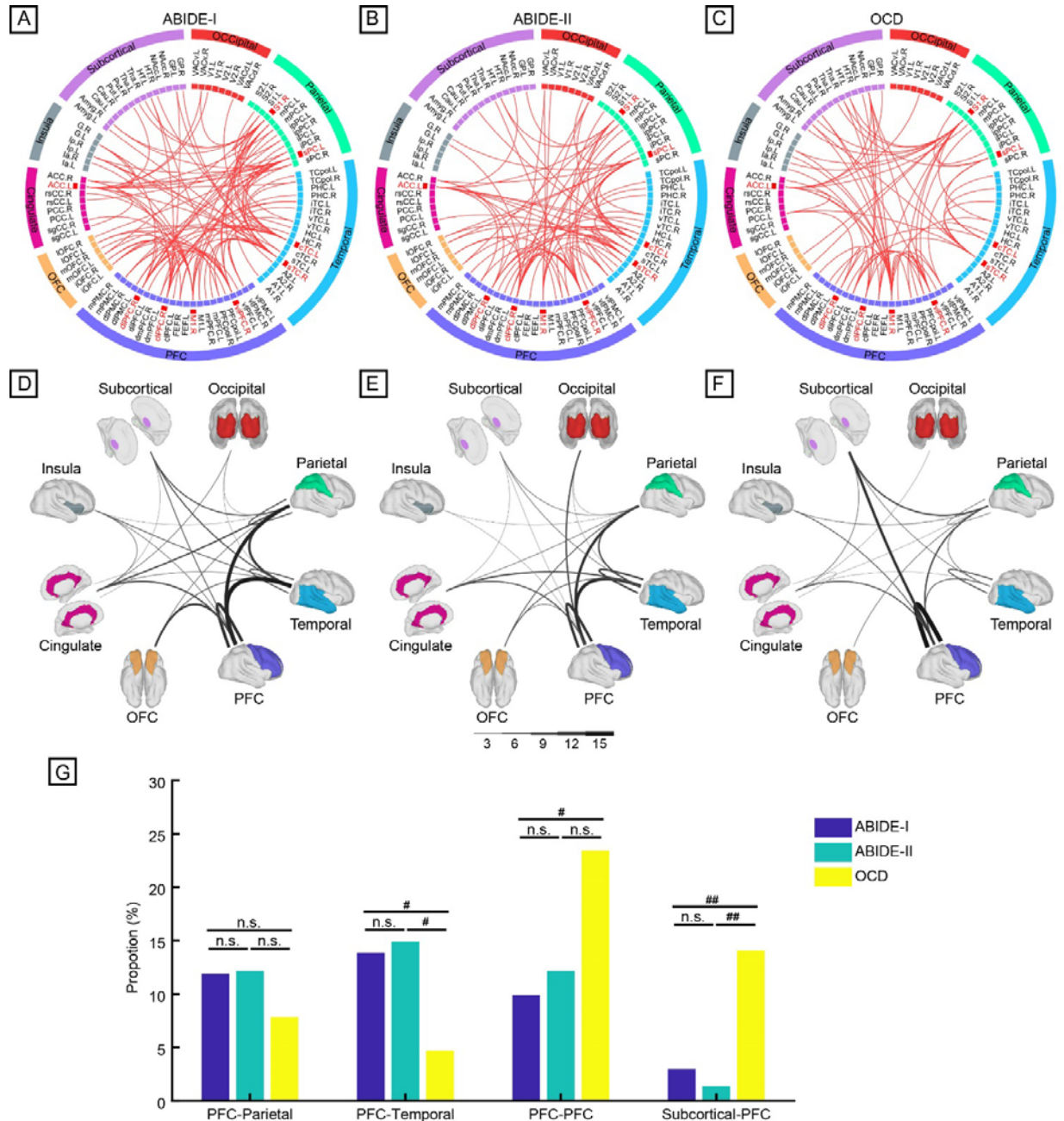
Fig. 3. Characteristic of the identified functional connections for ASD and OCD.

(A-C) The top row shows identified FCs and their terminal regions (nodes) for reliable distinguish

ASD from HCs and OCD from HCs. The inner layer denotes 94 brain regions, and the interlayer

highlights 9 core regions and the outer layer specifies the lobar division.

1   (D-F) Middle row shows the sum of the number of intra- and inter-lobe connection based on the lobar

2   division for ASD and OCD.

3   (G) Bottom row shows the comparison of intra- and inter-lobe connection with relative higher FCs

4   between ASD and OCD. # $p < 0.05$; ## $p < 0.01$uncorrected; n.s., not significant.
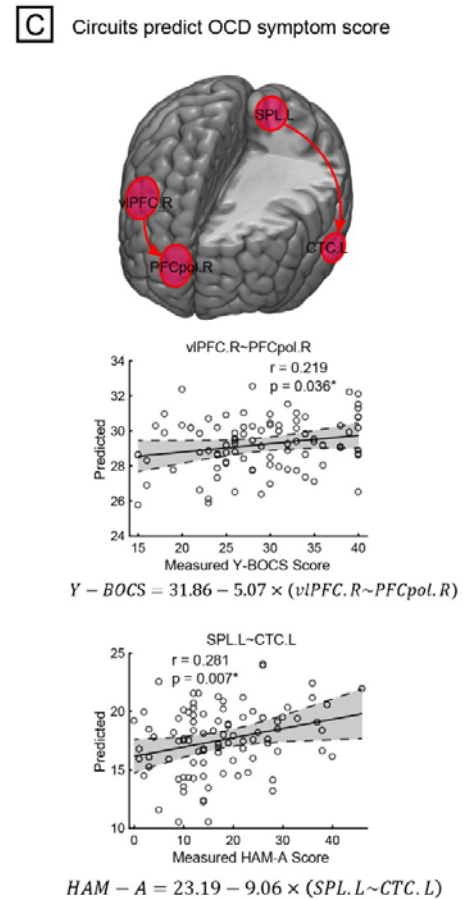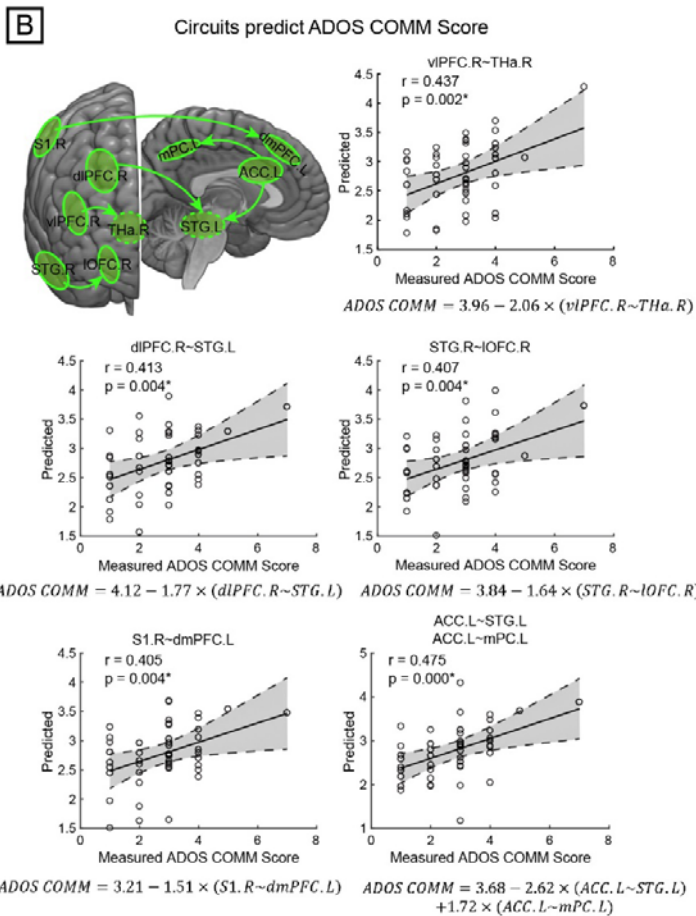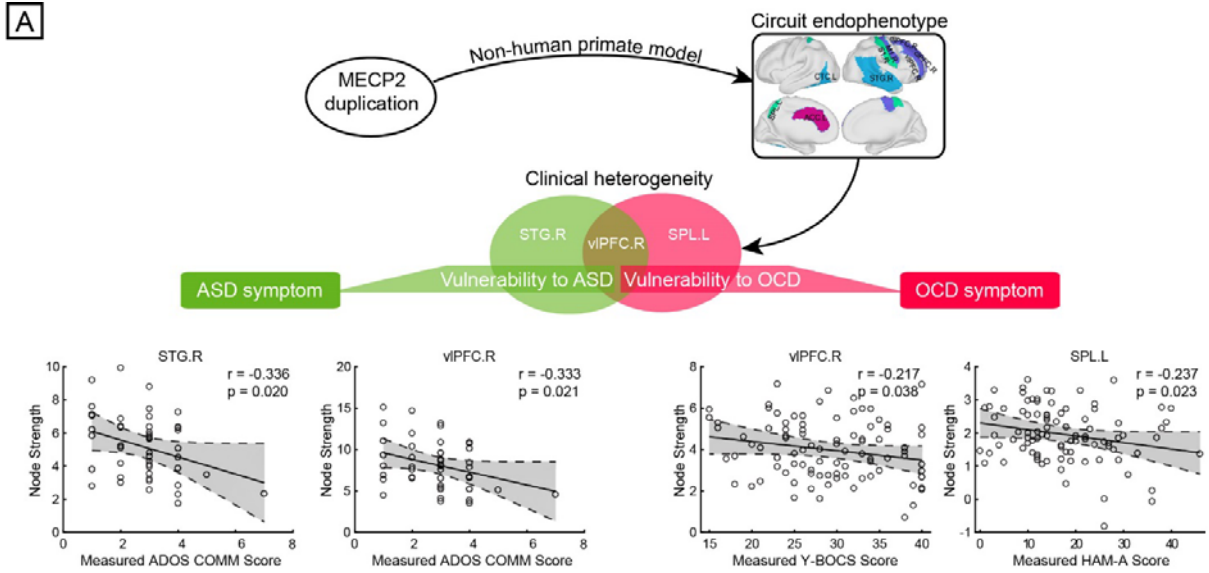
1   **Fig. 4. Genetically-linked neural circuits associated with distinct symptomatic**

2   **domains in ASD and OCD.**

3   (A) Effects of single genetic mutation in animal models can be limited to some specific neural

4   circuits (9 core regions) and associated behavioral manifestations in ASD and OCD. Node strengths

5   of the right vlPFC and right STG exhibited significant correlations with the ADOS COMM scores of

6   ASD patients, meanwhile the right vlPFC was found associated with Y-BOCS scores in OCD patients.

7   And the right SPL was correlated with their HAM-A scores.

8   (B) Predictions of ADOS COMM score based on linear models are shown at the bottom of each plot

9   for core regions including right vlPFC, right dlPFC, right STG, right S1, and left ACC. The

10   connection between the right vlPFC and right thalamus achieved a correlation of $r = 0.437$ ($p = 0.002$*)

11   between predicted and measured ADOS COMM score in ABIDE-II patients. Similarly, the measured

12   ADOS COMM score was predicted by the connections with right dlPFC and left STG ($r = 0.413$, $p =$

13   0.004*), right STG and right orbitolateral prefrontal cortex ($r = 0.407$, $p = 0.004$*), right S1 and left

14   dorsomedial prefrontal cortex ($r = 0.405$, $p = 0.004$*), and the connections between left ACC and both

15   left medial parietal cortex and left STG ($r = 0.475$, $p < 0.001$*), respectively.

16   (C) Predictions of Y-BOCS and HAM-A scores in OCD based on linear model are shown at the

17   bottom of plot for right vlPFC and left SPL. The connection between right vlPFC and right prefrontal

18   polar cortex was sufficiently strong to predict the actual Y-BOCS scores of patients ($r = 0.219$, $p =$

19   0.036*). The actual HAM-A scores of these OCD patients were significantly predicted by the FC

20   between left SPL and left CTC ($r = 0.261$, $p = 0.007$*). * indicates $p < .05$, FDR corrected. Shading

21   indicates a 95% confidence interval.